GDCh Research Article Angewandte International Edition Chemie www.angewandte.org

How to cite: *Angew. Chem. Int. Ed.* **2025**, *64*, e14543
doi.org/10.1002/anie.202514543

Cyclic Peptides

2D Assemblies Based on a Tetraphenylethylene D,L-Cyclic Peptide Scaffold

Alfonso Bayón-Fernández, Alba Torrón-Celada, Alejandro Méndez-Ardoy, Maëva Coste, David Delgado-Gestoso, Sébastien Ulrich, Javier Montenegro, and Juan R. Granja**

Abstract: Two dimensional (2D) materials and aggregation-induced emission (AIE) fluorophores have recently gained attention due to their unique properties and application potential. However, the combination of AIE probes into 2D self-assembled systems under nanometric control remains elusive due to the sensitivity of supramolecular assemblies to subtle changes in the monomer structure. Herein, we present a new scaffold based on four nanotube-forming cyclic peptide (CP) units attached to a tetraphenylethene (TPE) core whose pH-dependent self-assembly results in light-emitting 2D nanosheets. An oxime bond connection was exploited to synthesize a discrete library of tetrakis-(cyclopeptide) tetraphenylethene monomers that self-assemble into 2D macrotubular nanoarrays under the suitable external stimulus. This new tetrameric CP motif tolerates a broad range of molecular modifications, both on the peptide backbone and TPE core, without compromising the integrity of the 2D self-assembly. We also discovered that adjusting the molecular structure of the TPE aromatic core enabled precise height control of the supramolecular nanosheets. The alignment of the histidine residues within neighboring CPs allowed the application of 2D nanoarchitectures as enzyme mimics with esterase activity. The excellent tolerance to molecular diversity in both the external CP moiety and the internal aromatic AIE core, invites the design of new functional 2D supramolecular materials.

Introduction

Since graphene was discovered in 2004,[1] the development of new 2D materials has grown in importance due to their physicochemical properties.[2] The design of suitable synthetic methodologies is essential to tackle the obtention of well-defined materials with customized properties.[3] Interest in these materials is based on their unique properties, including their high morphological anisotropy, ultra-thin thickness, and a large surface area with numerous surface-active sites, along with other such as their unique electronic or magnetic properties. These characteristics make them promising candidates for use in applications such as catalysis, sensing, and energy conversion and storage. In the last years, molecular self-assembly has gained importance as it allows controlling the organization properties of nanostructures by encoding their information at the molecular level through the precise design of their basic building blocks.[4–6] A range of scaffolds such as peptides,[7–18] peptoids,[19–23] proteins,[24–31] nucleic acids,[32–37] polymers,[38–45] and others[46–49] have found applications on nanotechnology,[29,30,36,37] biology[14,16,22,23,31] or catalysis.[13,15,29] Peptides and proteins are of particular interest because they can be easily prepared by solid-phase or biotechnological strategies, they can be self-assembled according to their amino acid sequence, they are biocompatible and biodegradable,[50] and they can be combined with aromatic functional groups in hybrid biosupramolecular architectures.[51] Recently, we have unraveled the design parameters and potential structural requirements for the 1D to 2D self-assembly transition of nanotube forming cyclic peptides.[17,18] A number of oriented hydrophobic residues were required as noncovalent contact points for the aqueous assembly of bilayers or monolayers[52] of peptide nanotubes. A hydrophilic domain of ionizable residues (e.g., glutamic acids) balanced by neutral amino acids (e.g., histidine) was also required to avoid aggregation and maintain the aqueous

[*] Dr. A. Bayón-Fernández, A. Torrón-Celada, Dr. J. Montenegro, Dr. J. R. Granja
Centro Singular de Investigación en Química Biolóxica e Materiais Moleculares (CIQUS) and Departamento de Química Orgánica, Universidade de Santiago de Compostela, Rúa de Jenaro de la Fuente, s/n, 15705, Santiago de Compostela, Spain
E-mail: javier.montenegro@usc.es
juanr.granja@usc.es

Dr. A. Méndez-Ardoy
Department of Organic Chemistry and Instituto de Investigaciones Químicas (IIQ), CSIC, Universidad de Sevilla, C/Profesor García González 1, Avenida Américo Vespucio 49, Sevilla 41092, Spain

Dr. M. Coste, Dr. S. Ulrich
Institut des Biomolécules Max Mousseron (IBMM), CNRS, Université de Montpellier, ENSCM, Montpellier, France

D. Delgado-Gestoso
Department of Structure of Macromolecules, Centro Nacional de Biotecnología (CNB-CSIC), Darwin 3, Madrid 28049, Spain

Additional supporting information can be found online in the Supporting Information section

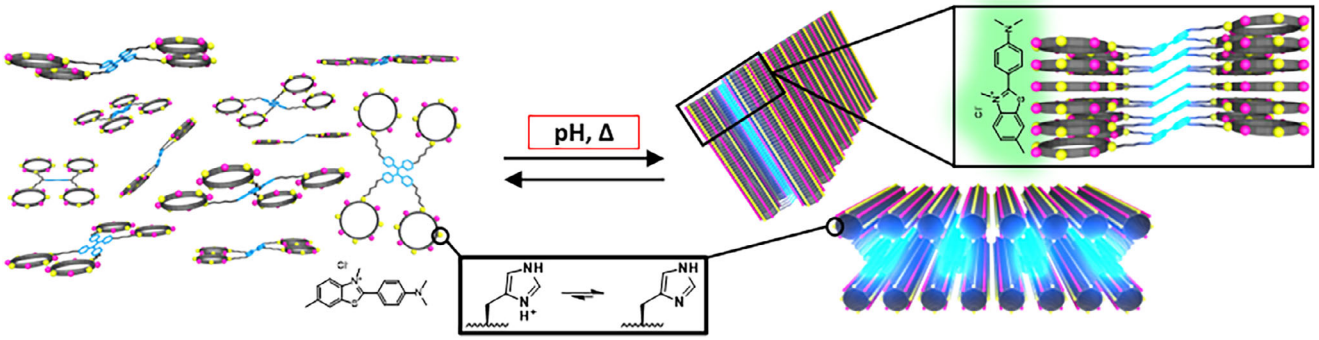

Figure 1. Schematic representation of the assembling into 2D nanosheets triggered by pH of model **4CP-U-TPE**.

integrity of ionized 2D supramolecular nanosheets. However, the stability of this 2D supramolecular assembly was sensitive to subtle modifications in the peptide sequence, particularly in the order and chemical nature of the hydrophilic amino acids that maintained the charge balance.[18] While these features conferred a dynamic character to these 2D systems from cyclic peptide monomers, new designs are called for the customized assembly of self-sustained tubular nanosheets with robust stability over a wide range of surface functional groups. Furthermore, these nanosheets lack of intrinsic fluorescent properties, therefore they require the addition of external fluorescent binding probes for their visualization.

Fluorescence emission of supramolecular aggregates can be achieved by the incorporation of aggregation-induced emission (AIE) probes. Tang et al. introduced this concept, using the 1-methyl-1,2,3,4,5-pentaphenylsilole.[53] While many of the commonly used dyes are susceptible to aggregation-caused quenching, the AIE chromogens exhibit weak luminescence in bulk solution, but their emission properties increase upon self-assembly.[54–56] The particular physicochemical properties of AIE probes[57] allow their implementation in various applications such as optoelectronics, biosensors, and smart materials.[54,57–62] One of the most used AIE dyes is the TetraPhenylEthene (TPE) due to its easy synthesis and incorporation of structural modifications, in addition to its emissive properties.[63] Over the years TPE derivatives have been incorporated to peptides,[64–70] polymers,[71–74] or other organic molecules.[75–81] A variety of different structures and materials have been developed, such as gels,[67–69,82] nanoparticles,[66,72,73,77] and cages,[69,72,75,83] that were then applied in sensing,[64,68,72,78–80,84–87] optoelectronics,[88] or imaging.[65,68,70,73,74,81] Over the years, several TPE-based smart hybrid systems have been shown to enable the assembly of supramolecular 2D nanostructures.[67,79,82,84,89,90] However, the supramolecular design potential and functional capacity of TPE aromatic cores that are substituted with complex organic scaffolds has yet to be discovered.

Herein we present a new synthetic design[91] for the robust 2D assembly of cyclic peptide nanotubes whose minimal structural unit (**4CP-U-TPE**) is based on a hydrophilic shell consisting of four cyclic peptides (CPs) that are connected to an aromatic TPE core through oxime bonds (Figure 1). The outer layer CPs surrounding the TPE core were selected with the idea of allowing pH-mediated control of their assembly. Both components, CPs and TPE are key in the supramolecular polymerization by establishing directional hydrogen bonds and π,π-interactions capable of guiding their hierarchical assembly into final 2D films. The versatility of this strategy in combining tetracarbonyl TPE scaffolds with alkoxyamine-equipped cyclic peptides allows molecular engineering of each component of this molecular hybrid without compromising their robust self-assembly into 2D architectures. Modifications to the peptide sequence, the aromatic core, or the length of their connectors can be applied to the preparation of robust nanosheets with nanometric control and customized chemical functionalities. These structures were characterized by atomic, electron and fluorescence microscopy, different spectroscopic techniques, and x-ray scattering showing the aqueous assembly of self-sustained large 2D supramolecular structures.

Results and Discussion

Molecular Design and Synthesis

CPs with an even number of alternating d,l-amino acids have the ability to self-assemble into nanotubes, known as self-assembly cyclic peptide nanotubes (SCPNs).[92] These structures are formed by staking different monomers on top of each other guided by the formation of a β-sheet type H-bonding networks along the tubular longitudinal axis. This versatile supramolecular structure allows the control of the nanotube diameter by adjusting the number and type of amino acids and external tubular properties according to the primary amino acids sequence. This fine control over the final structural properties permits their use as functional materials such as selective ion channels, tubular composites, or supramolecular antibiotics, among others.[93–95]

Previous studies of $\mathbf{CP_{1K}}$ scaffold (Figure 2) functionalized with different aromatic moieties showed its ability to self-assemble forming hydrogels under neutral or basic conditions. In this hierarchical process, peptide monomers are initially assembled into nanotubes whose aligned aromatic units are cluster and crosslinked to form fibers (SCPN bundles) capable to retaining water molecules within their structure to give rise to self-healing hydrogels.[96,97] The resulting

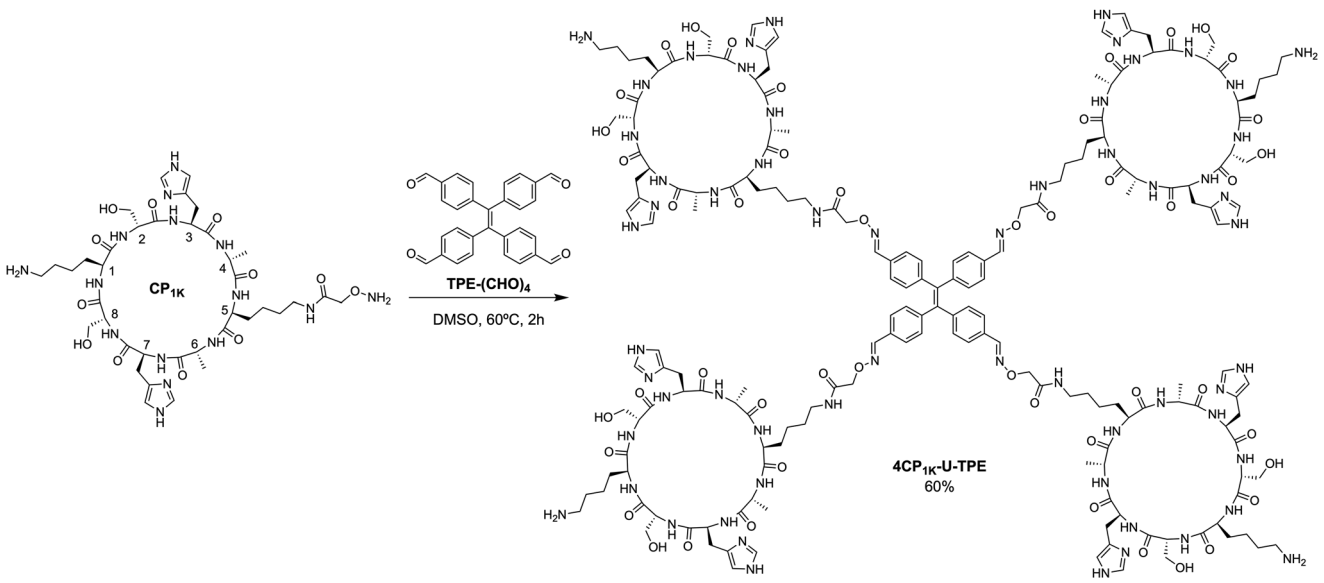

Figure 2. Synthetic scheme used in the preparation of **4CP$_{1K}$-U-TPE**.

fibers consist of a hydrophobic central core composed by the cluster of arene moieties surrounded by the assembled CPs.[98] Moreover, the supramolecular polymerization of pyrene derivative **CP$_{1K}$** in confined spaces can be spatially controlled by media conditions.[99] Unfortunately, the precise control of the fibrillar bundling process was challenging to achieve by the modulation of the relative spatial orientation of the aromatic moieties that bring together the SCPNs. In this sense and with the goal of creating fibers with a homogeneous diameter, we decided to design a novel building block that would allow to control the number of nanotubes (four in this case) surrounding the central hydrophobic core. To this end, we proposed to use of a tetrafunctionalized TPE derivative anchored by four cyclic peptides. Following this conceptual design, we selected the derivative **CP$_{1k}$** to anchor to the TPE derivative, which would resemble the central pyrene core of previous designs,[96,97,99] with the added advantage of an intrinsic aggregation-triggered fluorescent emission upon self-assembly. Thus, the alkoxyamine-equipped cyclic peptide **CP$_{1K}$** was prepared by Fmoc solid phase peptide synthesis as previously reported[96] and then condensed with the TPE derivative containing four *para*-oriented carbaldehyde moieties (**TPE-(CHO)$_4$**),[90] by heating at 60 °C in DMSO for 2 h to provide **4CP$_{1K}$-U-TPE** (Figure 2). After the oxime bond formation, HPLC-MS, ^{1}H NMR, and IR spectroscopy characterization confirmed the proposed structure and purity of the final molecule (Figure S68–S70).

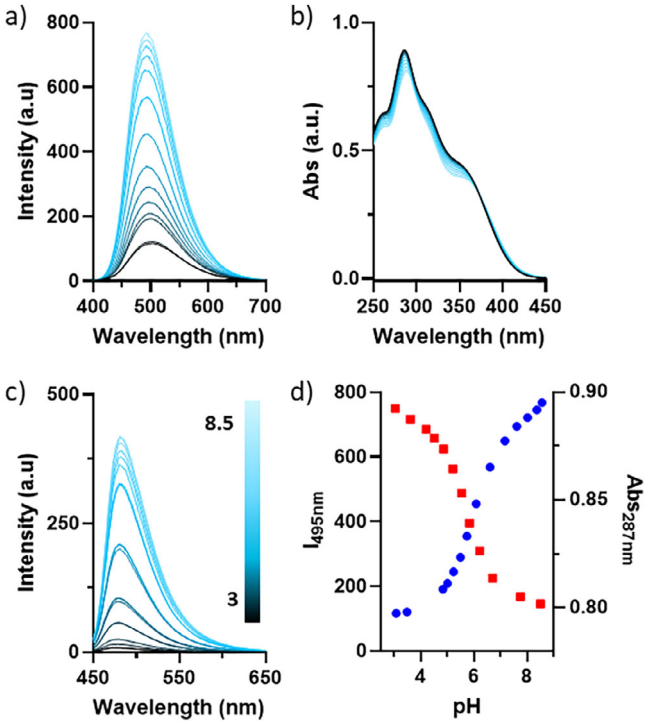

Figure 3. Spectroscopic characterization of **4CP$_{1K}$-U-TPE** (50 μM) in aqueous media at different pHs. a) Fluorescence spectra (λ_{exc} = 365 nm); b) UV-vis spectra; c) Fluorescence spectra of ThT (10 μM) in presence of the peptide (λ_{exc} = 440 nm), and d) changes on maximum emission (I_{max} = 495 nm, blue dots) and absorbance wavelength (Abs_{max} = 287 nm, red squares) with pH.

Alkalinization of 4CP$_{1K}$-U-TPE Triggers Its Self-assembly and Emission

To understand the self-assembly capabilities of **4CP$_{1K}$-U-TPE**, we performed pH titrations monitoring spectral changes through fluorescence and UV–vis spectroscopy (Figure 3). Alkalinization of an aqueous solution of **4CP$_{1K}$-U-TPE** (50 μM, pH 3) resulted in the expected increase in fluorescence emission at 495 nm (λ_{exc} = 365 nm, Φ_f = 16.1%, τ = 2.0 ns) with a slight blueshift of the maximum, which can be attributed to the stacking of the aromatic rings and the consequent inhibition of the rotation of the phenyl groups of the dye (Figure 3a, Figure S1a–f).[55,63] UV absorption

profile showed a redshift of the absorbance maximum and a slight decrease in absorbance, compatible with the packing of the TPE moieties (Figure 3b, Figure S1b).[79] To verify whether the emission of the AIE dye was concomitant with the formation of β-sheet structures and therefore, with the formation of SCPNs, pH titrations in the presence of Thioflavin T (ThT) and WAXS measurements of the freeze-dried product were carried out.[17] ThT is the gold-standard in the detection of amyloid fibrils, due to its ability to stain "cross-β" structures.[100,101] Insertion of the dye increases its fluorescence emission and induces a red shift of the absorbance maximum from 412 up to 440 nm. As expected, basification of **4CP$_{1K}$-U-TPE** solution to pH 8.5 in the presence of the dye resulted in a 50-fold increase in the fluorescence intensity, accompanied by the characteristic red shift (412 to 440 nm) in the absorbance spectrum (Figure 3c, Figure S1c). Overall, these results and the observed WAXS spacings between 4.2 and 4.7 Å (Figure S1g) confirm the concomitant assembling of both TPE and CPs units. When plotting the fluorescence emission at 495 nm (I_{max}) or the maximum absorption (Abs_{max}) as a function of pH, a clear transition around pH 6 is observed (Figure 3d). This supports that histidine deprotonation ($pK_a \sim 6$) drives the supramolecular polymerization. At the final titration point (pH 8.5), the lysine side chains are partially protonated and strongly solvated, thus preventing the system from further aggregation through CPs interdigitation.[102]

The reversibility of the assembly with pH and temperature was then addressed. Initially, reversibility was addressed with pH (Figure S2a) and afterwards, the influence of temperature was verified at pH 6 and 8, conditions at which the system was already assembled (Figure S2b and c). In both cases, the system showed full reversibility with almost complete quenching of the TPE emission when heated to 90 °C for a few minutes or subjected to acidic conditions. At pH 2, although the tetrameric compound disassembled, it was unfortunately unstable as it underwent partial hydrolysis of oxime bonds, which prevented further studies. At pH greater than 6 there are no notable differences in the estimated values of Critical Assembly Concentrations (CAC), although it appears that at pH 8 the fluorescence intensity was higher, suggesting that the system is in a higher assembled state (Figure S3).

Microscopy Reveals the Presence of Large 2D Assemblies

In sharp contrast with our expectations, the alkalinization of the **4CP$_{1k}$-U-TPE** solution did not result in the formation of well-defined fibers consisting of four parallel nanotubes that are entangled by water molecules to lead to sol-gel transitions. Instead, solutions of **4CP$_{1K}$-U-TPE** at concentrations above its CAC gave rise to microscopic 2D supramolecular assemblies that were characterized using different microscopic techniques (Figure 4).

As already determined by spectroscopic techniques, **4CP$_{1K}$-U-TPE** retains the AIE properties of the TPE moiety. Epifluorescence microscopy of alkaline solutions (20 mM HEPES, pH 8) showed a continuous fluorescent layer extending over large areas of the sample (Figure S4). In some areas, different cracks and fractures appeared in the films, most likely as a consequence of the friction caused during the deposition process (Figure S5a and smaller sheets in Figure S5b), confirming the formation of long films of 100 μm^2. To further confirm that these fluorescent layers corresponded to the large-sized sheets, these samples were mechanically scraped with a pipette tip or shaken vigorously, resulting in the appearance of smaller sheets as a result of their breakage (Figure 4a, Figure S6, Video S1). The addition of ThT to this solution resulted in an emission overlap (Figure 4b, Figure S7), with the sheets emitting at the characteristic wavelength of the external dye, suggesting that the sheets are formed by assembled nanotubes that grow laterally to form the 2D structures. This lateral assembly pattern may also explain the 3.2 and 2.5 Å spacings obtained by WAXS (Figure S1g). These distances are characteristic of β-sheet structures but are also found in other types of peptide aggregates.[52,103,104]

Scanning transmission electron microscopy (STEM) images (Figure 4c, Figure S8) again confirmed the presence of the 2D structures in which sharp boundaries and folded edges could also be observed. To accurately measure the height of the sheets, aliquots of the aqueous solution of **4CP$_{1K}$-U-TPE** (20 μM) were deposited on mica surfaces and studies by AFM. Noncontact AFM micrographs revealed the presence of long sheet-like structures with an average height of 3.7 ± 0.2 nm, which correspond quite well with the dimensions of two stacked nanotubes separated by the TPE moiety (Figure 4d, Figure S9). Unmodified octa-CPs previously reported in the literature had heights of around 1.6 nm for a single SCPN and 3.2 nm for the bilayers,[17] while CPs containing a pyrene anchored on the side chain of a Lys of a CP forming SCPNs could reach 2.5 nm.[96] Taking these values as reference, we expected that our molecule could form nanotubes with a height of approximately 4 nm. In any case, it should be noted that the aromatic moiety must most likely be slightly tilted with respect to the plane defined by the CPs to compensate for the smaller distance between the stacked arenes (~3.5 Å) than between the CPs (~4.5 Å).[98] Therefore, the observed height coincides quite well with that estimated for the proposed structure (Figure 5a,b). Similarly, 2D materials were also obtained at lower pH (pH 6, 20 mM MES, Figure S10). Finally, cryo-microscopy was also performed to confirm the formation of nanosheets in solution and to rule out self-assembling growth mediated by the surface. Images taken from a 20 μM solution of **4CP$_{1k}$-U-TPE** (20 mM HEPES, pH 8, Figure 4e and f and Figure S8b) again showed large, sheet-like surfaces partially covering the grid. However, some small plates were also present, likely resulting from the rupture of the larger sheets. Interestingly, in addition to these large nanosheets, short nanotubes (20–70 nm) with diameters of ~6.0 nm were also observed (Figure 4g and Figure S8b). Composed of approximately from 50 to 150 CPs, these short nanotubes could represent the intermediate building block in the hierarchical growth of supramolecular nanosheet. Dynamic simulations have previously demonstrated this two-steps process, showing that, once the nanotubes reach a certain length, lateral contacts are favored promoting 2D growth over longitudinal elongation.[52]

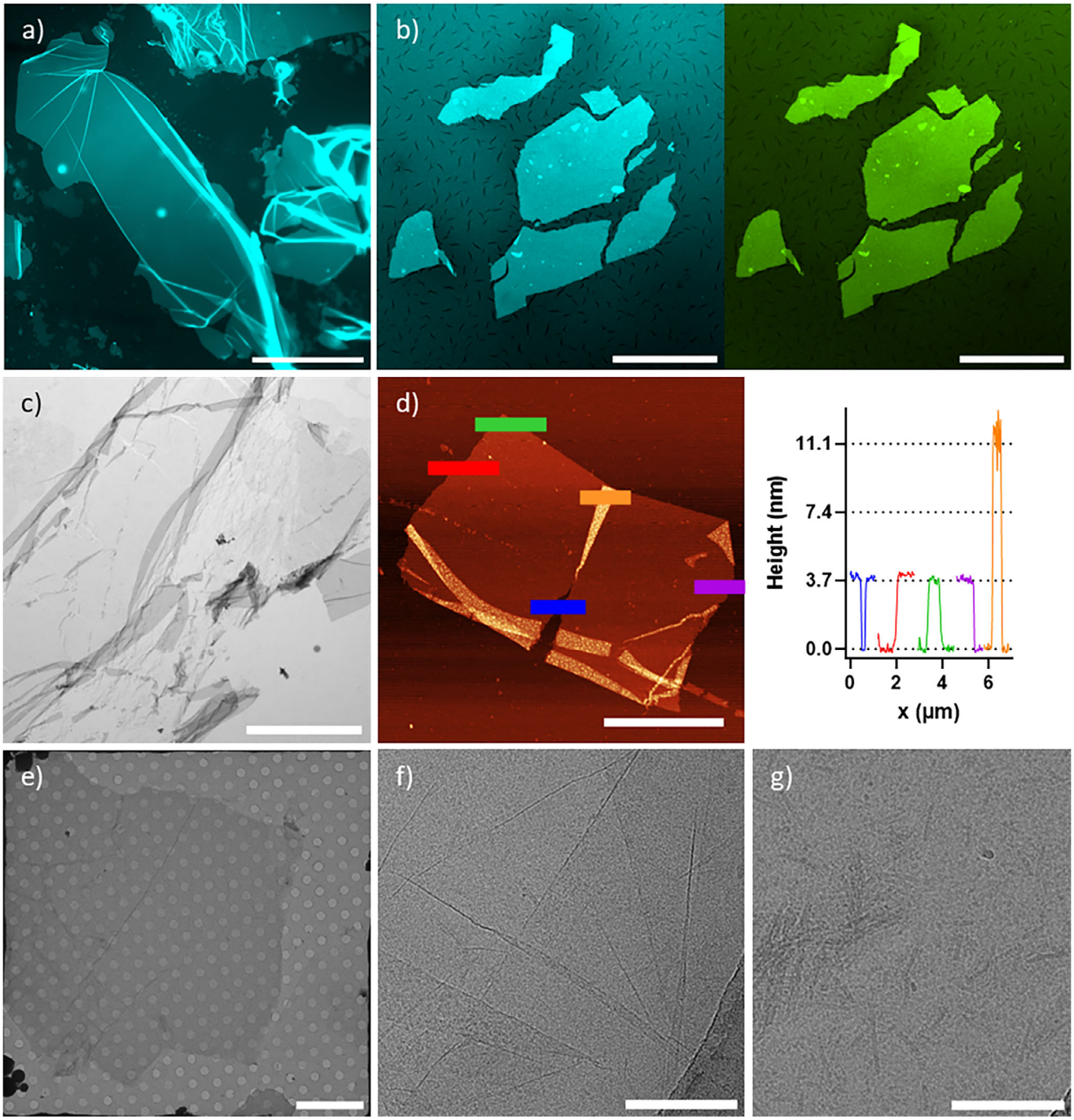

Figure 4. Images obtained from the characterization of an aqueous solution of **4CP$_{1k}$-U-TPE** (20 μM) in HEPES (20 mM, pH 8) showing the presence of sheet-like structures. a) Epifluorescence image (scale bar 200 μm); b) Epifluorescence picture of this solution in the presence of ThT (10 μM) (scale bar 100 μm); c) STEM (scale bar 4 μm); d) AFM micrograph on the left (scale bar 3 μm) and height profile on the right; e-g) Cryo-TEM microscopy showing a big sheet, sheet folds and SCPNs respectively (scale bar 10 μm for e and 100 nm for f and g).

Scaffold Versatility and Height Control to Form 2D Structures

Considering the pH dependence on the self-assembly process, we proposed a hierarchical mechanistic model based on the initial formation of four nanotubes bundles, in which hydrogen bonding interactions and TPE stacking direct the assembly mode (Figure 5a and b). The presence of the very short nanotubes in cryo-microscopy images confirms the existence of these intermediates. We believe that, once they reach a minimum size, they begin spreading laterally. As a consequence of the pairing between His, the four resulting nanotubes are arranged into two pairs, leaving the stacked TPE moieties located between these nanotube pairs. On both sides of these pairs of nanotubes there are still imidazole rings along the SCPNs with the ability to continue interacting with other nanotube tetramers to induce their lateral growth

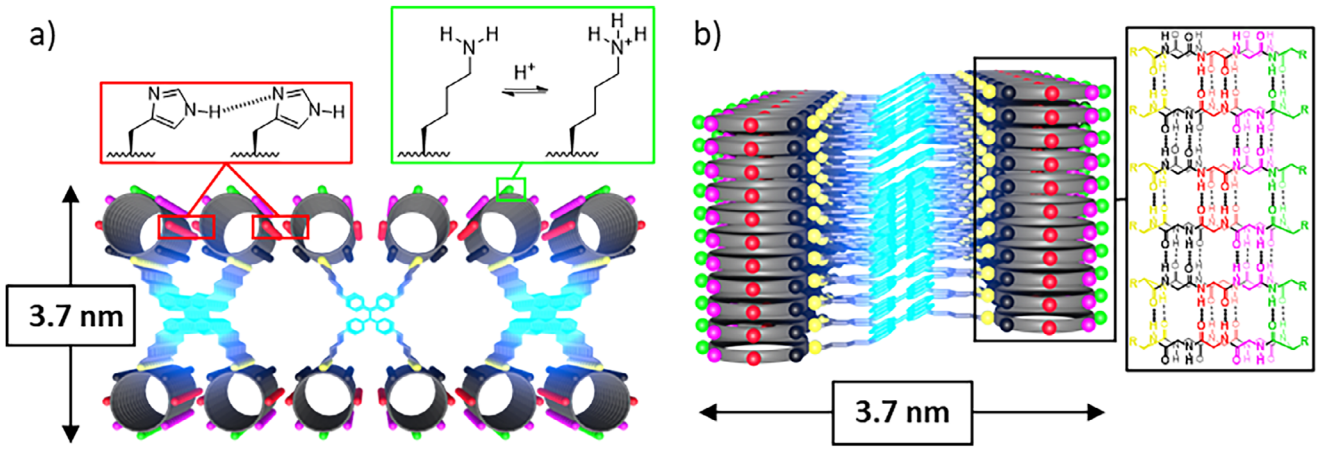

Figure 5. Schematic representations of the proposed assembling mechanism used different colors to indicate the type of amino acids. Green represents lysine side chain, magenta represents serine, red represents histidine, black represents alanine, and yellow represents the lysine involved in the connection with TPE. a) Top view of the proposed model of the sheet formed by the assembly of **4CP$_{1K}$-U-TPE**. The squares highlight properties contributed by some of the residues, such as the His–His pairing. This is marked by a hydrogen bond between the two rings. However, other types of interactions are also possible, such as π–π stacking.[105,109] The cationic properties of the sheets are modulated by changes in the protonation state of the Lys side chain with the pH. b) Side view illustrating the tilt of the TPE moieties with respect to the CPs assembly. On the right is the structural model of one of the peptide nanotubes, in which the cyclic peptides are stacked by forming β-sheet-type hydrogen bonding interactions. The same color code is used to differentiate the different residues.

and prevent the exposure to the aqueous medium of the hydrophobic central layer formed by the TPE stack and in this way give rise to the corresponding solvated laminas in which the lysine side chains are exposed on their surface, protecting them from further aggregation (Figure 5a). This model is also supported by the way these sheets break (Figure S24c), resulting in narrow nanosheets and frequently, linear edges with right-angled corners. This is more typical of the lateral growth of nanotubes than other models, such as the interdigitation of CPs of different monomers. In the latter case, these sheets would break preferentially in one direction.

With the aim of unveiling the lateral growth mechanism that promotes the enlargement and stability of these bidimensional assemblies, we decided to make different modifications in amino acids of the peptide sequence identified as key (Table 1, entry 1–10, Figure 6a–i) as well as in the TPE that forms the hydrophobic central core (Table 1, entry 11–13, Figure 6j–l), according to our mechanistic proposal for hierarchical assembly (Figure 5a,b). To check the importance of the positive charge of the canonical lysine, we substituted the former for glutamine (uncharged) or glutamic acid (acid). The role played by the histidine and its position in the CP sequence and protonation stage were also evaluated, for which we permuted or changed this residue for others. In addition, the relevance of the connector length between CP and TPE moiety was also evaluated by reducing its length, replacing Lys with 2,3-diaminopropionic acid (Dap).

Once the mentioned CPs were prepared (for details on the sequences and synthesis, see the Supporting Information) and condensed with the TPE moiety the formation of 2D-structures was evaluated in a similar manner to the original precursor (Figure 6, Figure S11, S22). To our surprise and satisfaction, most of the new derivatives provided 2D structures again, although some key features should be mentioned.

Table 1: Structural modifications of **4CP-U-TPE** scaffold. Aa substitutions and TPE modifications are shown in red with respect to **4CP$_{1K}$-U-TPE**, alterations in amino acid positions are denoted in green while chirality alterations are denoted in pink. The number used to indicate the position occupied by each Aa can be seen in 2.

Entry	Name	1	2	3	4	5	6	7	8
1	**4CP$_{1K}$-U-TPE**	K	S	H	A	K-Oxime-4-TPE	A	H	S
2	**4CP$_{1Q}$-U-TPE**	Q	S	H	A	K-Oxime-4-TPE	A	H	S
3	**4CP$_{1E}$-U-TPE**	E	S	H	A	K-Oxime-4-TPE	A	H	S
4	**4CP$_{2,8H}$ -U-TPE**	K	H	S	A	K-Oxime-4-TPE	A	S	H
5	**4CP$_{4,6H}$ -U-TPE**	K	S	A	H	K-Oxime-4-TPE	H	A	S
6	**4CP$_{6,8H}$ -U-TPE**	K	S	A	A	K-Oxime-4-TPE	H	S	H
7	**4CP$_{3A}$-U-TPE**	K	S	A	A	K-Oxime-4-TPE	A	H	S
8	**4CP$_{7R}$-U-TPE**	K	S	H	A	K-Oxime-4-TPE	A	R	S
9	**4CP$_{H(Me)}$-U-TPE**	K	S	H(Me)	A	K-Oxime-4-TPE	A	H(Me)	S
10	**4CP$_{5Dap}$-U-TPE**	K	S	H	A	Dap-Oxime-4-TPE	A	H	S
11	**1CP$_{1K}$-U-TPE**	K	S	H	A	K-Oxime-1-TPE	A	H	S
12	**4CP$_{1K}$-U-TPE$_{OH}$**	K	S	H	A	K-Oxime-4-TPE(OH)	A	H	S
13	**4CP$_{1K}$-U-TPE$_{PEG}$**	K	S	H	A	K-Oxime-4-TPE(PEG)	A	H	S
14	**4CP$_{QRS}$-U-TPE**	R	S	H	A	K-Oxime-4-TPE	A	H	Q
15	**4CP$_{QSR}$-U-TPE**	S	R	H	A	K-Oxime-4-TPE	A	H	Q
16	**1CP$_{QRS}$-U-B**	R	S	H	A	K-Oxime-Benzene	A	H	Q
17	**1CP$^{5L}_{QRS}$-U-B**	R	S	H	A	K-Oxime-Benzene	A	H	Q

The replacement of the Lys by a Gln (**4CP$_{1Q}$-U-TPE**, entry 2), gave rise to structures with similar morphologies (Figure 6a, Figure S11) although precipitating at higher pH, as could be expected for this modification (Figure S11b). This confirms the importance of protonation of lysines on the surface of the sheets to keep them solvated in solution at broader pH ranges and prevent their uncontrolled aggregation. On the other hand, its substitution by a Glu (**4CP$_{1E}$-U-TPE**, entry 3) promotes the disassembly of laminas at pH higher than 6.5 (Figure 6b, Figure S12), thus, narrowing the assembly to precise pH ranges. This might be caused

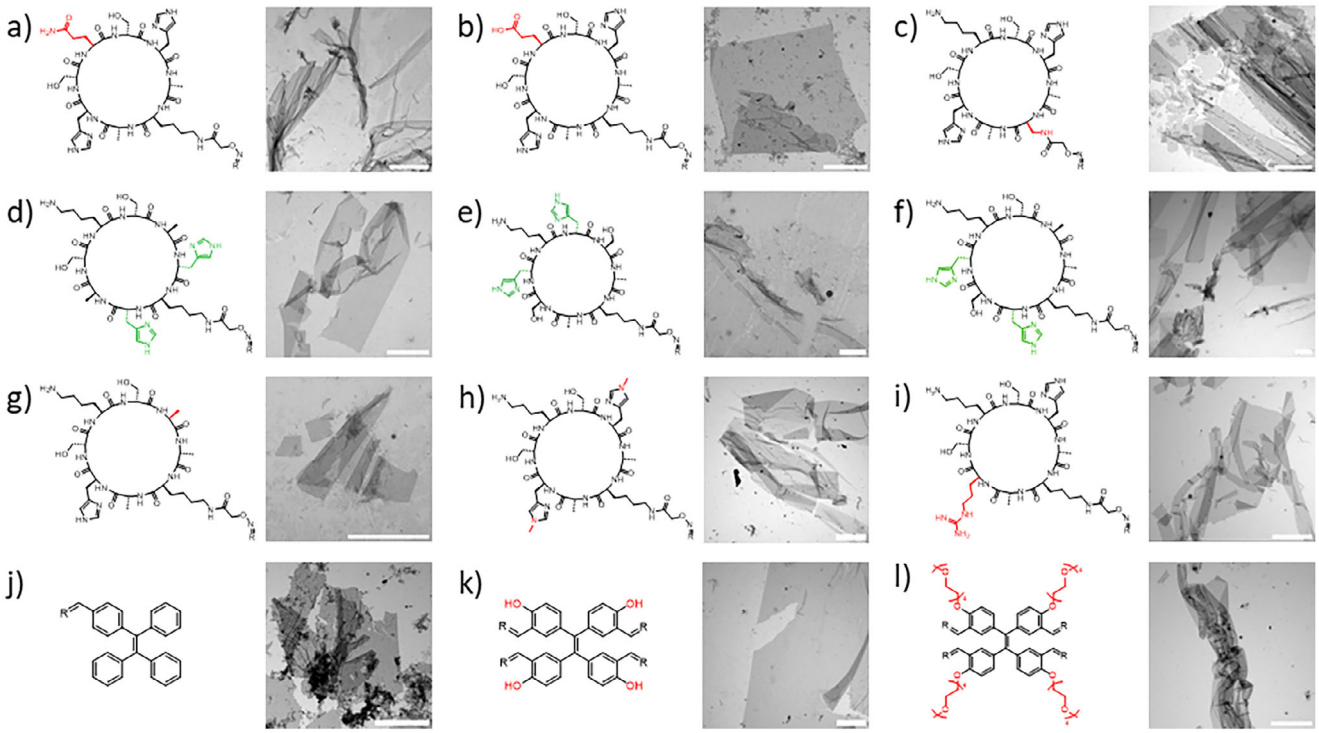

Figure 6. Partial chemical structure showing structural changes with respect to the initial structure (**4CP$_{1K}$-U-TPE**) and STEM showing sheet like structures at 50 μM for a) **4CP$_{1Q}$-U-TPE**, b) **4CP$_{1E}$-U-TPE**, c) **4CP$_{5Dap}$-U-TPE**, d) **4CP$_{4,6H}$ -U-TPE**, e) **4CP$_{2,8H}$ -U-TPE**, f) **4CP$_{6,8H}$ -U-TPE**, g) **4CP$_{3A}$-U-TPE**, h) **4CP$_{H(Me)}$-U-TPE**, i) **4CP$_{7R}$-U-TPE**, j) **1CP$_{1K}$-U-TPE**, k) **4CP$_{1K}$-U-TPE$_{OH}$**, and l) **4CP$_{1K}$-U-TPE$_{PEG}$**. Scale bars are 3 μm, pH 6 (a, b and k) and pH 7-8 (rest of the samples).

by the increasing repulsion between negatively charged carboxylates of neighboring stacked CPs once both His are deprotonated. Moreover, two sets of modifications were carried out on histidine at positions 3 and 7. As mentioned above, the proposed hypothesis was that these residues, once partially deprotonated, could promote the lateral growth of **4CP$_{1K}$-U-TPE** nanotubes though the formation of multiple H-bonds, most likely mediated by water molecules, with other nanotubes.[105–109] The first set of modifications consisted of exchanging the positions occupied by His with other residues in the CP sequence. Therefore, they were switched with Ser (**4CP$_{2,8H}$-U-TPE**, entry 4) or with Ala (**4CP$_{4,6H}$-U-TPE**, entry 5), and additionally, another derivative was also prepared in which both His were placed on the same side of the macrocycle, breaking the pseudosymmetric distribution on both sides of the axis defined by the Lys$_{1,5}$ (**4CP$_{6,8H}$-U-TPE**, entry 6). None of these changes led to significant variation in the morphology of the 2D-structures (Figure 6d–f, Figure S14–S16). The second set of modifications consisted of the replacement of one or both His by other residues with different properties. To avoid or reduce the aforementioned lateral hydrogen bonds as propagators of lateral growth, His$_3$ or His$_7$ were substituted, respectively, by an Ala (**4CP$_{3A}$-U-TPE**, entry 7), a small and nonpolar residue, or by an Arg (**4CP$_{7R}$-U-TPE**, entry 8), a positively charged residue that, in principle, should increase the lateral electrostatic repulsions between tubes. Additionally, both His were replaced by the *H-N*-3-Methyl-L-histidine derivative (**4CP$_{H(Me)}$-U-TPE**, entry 9) in order to reduce their hydrogen bond donor ability. To our surprise, all peptide derivatives behaved similarly (Figure 6g–i, Figure S17–S19), again forming the corresponding 2D structures, suggesting the predominant role that hydrophobic assembly of the TPE units plays also in lateral 2D spreading. Interestingly, **4CP$_{7R}$-U-TPE** derivative provided emitting films whose stability was maintained throughout the pH range studied. We attributed this to the presence of the charged Arg side chain, which could also be involved in the lateral growth through cation-π interactions or the formation of hydrogen bonds with the surrounding imidazole moieties. In summary, all modifications of cyclic peptides yielded in robust 2D supramolecular assemblies, whose pH sensitivity could be tuned by subtle changes in the amino acid sequence without altering their ability to form such materials – for example: **4CP$_{1K}$-U-TPE** (5.5–11), **4CP$_{1Q}$-U-TPE** (5.5–6.5), **4CP$_{1E}$-U-TPE** (5.5–7), and **4CP$_{7R}$-U-TPE** (6–12.5).

Additionally, to reduce the flexibility of the tetrakis-(cyclopeptide)TPE precursors, the Lys used for the connection to the TPE was replaced by a Dap (**4CP$_{5Dap}$-U-TPE**, entry 10), thereby reducing the length of the linkers by three carbons. Once again, this modification did not provide any significant change on the self-assembling properties, giving rise to aggregates similar to those observed for **4CP$_{1K}$-U-TPE** (Figure 6c, Figure S13). As expected, the reduction of the length of the connectors between the CPs and the TPE resulted in thinner sheets with an average height of 3.2 ± 0.3 nm (Figure 7, Figure S13e).

To study the structural tolerance of the aromatic core, three different TPE derivatives were also studied. First,

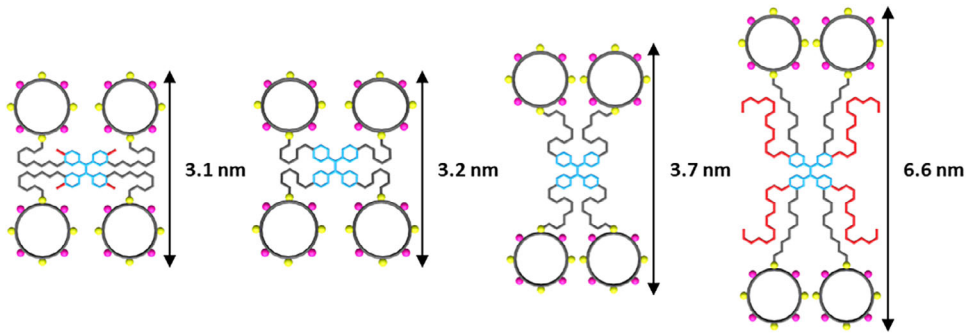

Figure 7. Scheme representing how the CP distribution along the TPE core can explain the height differences observed by AFM experiments. From left to right: **4CP$_{1K}$-U-TPE$_{OH}$**, **4CP$_{5Dap}$-U-TPE**, **4CP$_{1K}$-U-TPE**, and **4CP$_{1K}$-U-TPE$_{PEG}$**.

a monosubstituted TPE derivative, **TPE-(CHO)$_1$** was condensed with **CP$_{1K}$** to form control model **1CP$_{1K}$-U-TPE** (entry 11). This derivative was designed with the aim of leaving the TPE moiety exposed to the solvent as in the previous pyrene precursor[96,97,99] while breaking the C4 symmetry of the tetra substituted derivative. STEM analysis of solutions of this CP (50 μM) showed the coexistence of both sheets and small fibers that could correspond to SCPNs or bundles of them (Figure 6j, Figure S20). Analysis of AFM micrographs of these samples provided the height of these layers, which had an average height of 8.2 ± 0.8 nm, much higher than those obtained with the tetrakis-derivatives, suggesting a different assembly pattern, for which we propose a multilayer assembly pattern (Figure S20d, Figure S23). This assembly promiscuity for the TPE mono-adduct supported the importance of the tetrameric template to bias the self-assembly towards 2D supramolecular systems. Next, we employed the phenolic derivative of TPE (**TPE$_{OH}$-(CHO)$_4$**) to form **4CP$_{1K}$-U-TPE$_{OH}$** (entry 12) whose connection with the CPs would be to meta-oriented oximes and would give rise to assemblies with a central core with less hydrophobic character. This analogue also led to the formation of slightly thinner 2D plates (3.1 ± 0.1 nm, Figure S21), which already begin to disassemble under neutral conditions (e.g., pH > 6, see Figure 6k, Figure 7, Figure S21). These results with a meta-oriented tetraphenolic core confirm the robust 2D templating effect of the tetrasubstituted TPE moieties even when less hydrophobic central cores are used and therefore, should have a lower tendency for lateral aggregation of the SCPN tetramers. Finally, a pegylated derivative of the TPE unit was also prepared (**4CP$_{1K}$-U-TPE$_{PEG}$**, entry 13) and once again 2D sheets were also obtained. In this case, the resulting supramolecular nanoplates were stable at pH above 6, suggesting that the aforementioned disassembly of the non-PEGylated derivative must be related to the deprotonation of phenol. The thickness of the resulting lamellae, as confirmed by AFM is affected by these modifications in the central core of the TPE, presenting an average height of 6.6 ± 0.3 nm, approximately 1.8 times thicker than the original structure (Figure 6l, Figure 7, Figure S22). This significant increase in height is consistent with an expansion of the central hydrophobic core due to the presence of the tetraethylene glycol chains occupying spaces in the central part of the bilayer, but without apparently affecting 2D lateral growth. In general, all the different designed cyclic peptide scaffolds showed similar morphology and spectroscopic properties, only differing according to peptide sequence or TPE substitution (e.g., Gln, Glu, and **TPE$_{OH}$** derivatives) in their stability with the pH of the medium or the height of the supramolecular sheets. Therefore, all the tetrapeptide derivatives studied form monolayers whose height can be meticulously modulated by key modifications in the length of the connectors or in the central aromatic moiety, forming sheets whose thickness range from 3.1 nm to 6.6 nm (Figure 7)

Given the ability of these tetramers to form 2D structures, we measured the melting temperatures of some of these materials to clarify the formation mechanism and evaluate their inter-tubular interactions during nanotube lateral growth. We focused on residues arranged orthogonally (3 and 7) to the TPE connection, specifically His. To this end, we studied the derivatives **4CP$_{1K}$-U-TPE**, **4CP$_{3A}$-U-TPE**, and **4CP$_{2,8H}$-U-TPE**. Peptide derivative **4CP$_{3A}$-U-TPE** has only one His because the second was substituted with an Ala; therefore, the number of interactions between these residues is reduced by half. Conversely, **4CP$_{2,8H}$-U-TPE** has two histidine-oriented outward. According to our model, the imidazole rings are farther apart, so, inter-histidine interactions are replaced by interactions between the hydroxyl groups of Ser.

As shown in Figure S2d, these changes drastically modify the stability of the sheets. The most stable nanosheets are those derived from the original tetramer (**4CP$_{1K}$-U-TPE**). As expected, eliminating one of the histidines reduces the stability of the supramolecular sheet. The least stable 2D structures result from CPs with His residues that are most exposed to the aqueous medium (**4CP$_{2,8H}$-U-TPE**). These results clearly demonstrate that inter-tubular interactions and hydrophobic effects generated by TPE stacking contribute to the lateral growth of nanotubes.

Catalytic Activity

In the proposed final assembled structure, the imidazole rings in the layer covered by the assembled cyclopeptide units would be exposed, at least partially to the aqueous interphase. These spatial arrangement of the imidazole rings

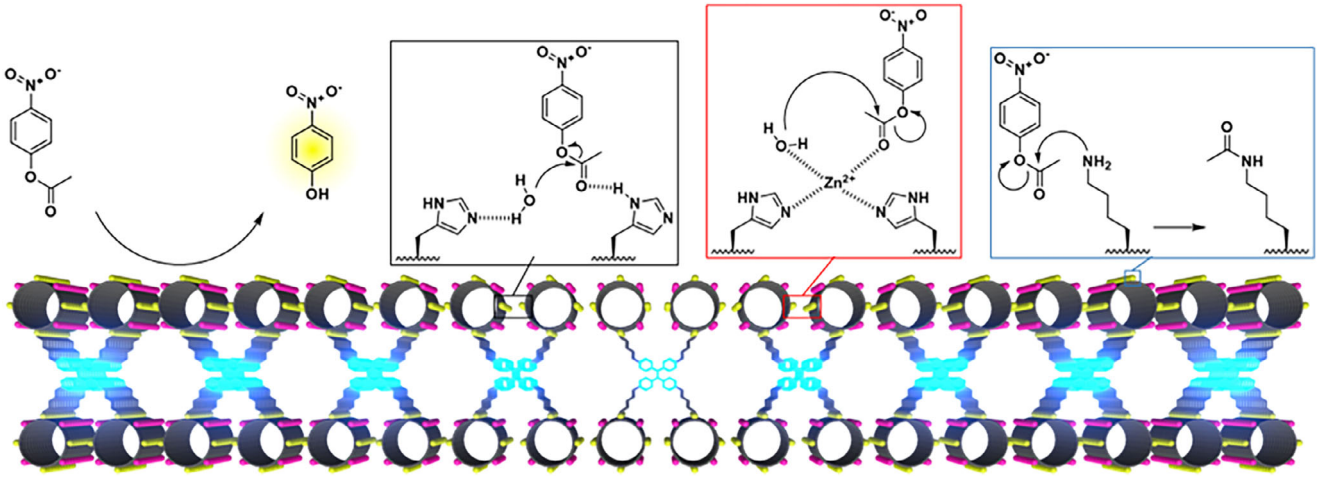

Figure 8. Scheme representing the catalytic activity of the CP based sheets and the mechanism of the histidine mediated (black) and metal mediated (red) catalysis. In blue it is represented the possible mechanism of the lysine acetylation.

on the surface provides an excellent opportunity to test their ability to induce esterase-type reactions, as has been shown for other types of aggregates, especially unidimensional ones, such as fibers or gels.[110–114] Furthermore, this alignment along the nanotube, together with the proximity of other imidazole rings from neighboring nanotubes, could provide a suitable environment not only for their participation in the proposed acid/base proton transfer processes but also lead to carbonic anhydrases-like activity, in which these heterocycles would coordinate with a suitable metal center, such as zinc. This coordination would provide additional evidence of lateral nanotube growth during the 2D structures formation. As previously mentioned, this growth is supported by the hydrophobic effects related to the central TPE core and the interactions between the side chains, particularly His residues. Coordination of Zn^{2+} ions confirmed that they do not affect the 2D morphology (Figure S24a). EDX-TEM experiments (Figure S24b) clearly demonstrate the deposition of this ion on the sheets. After established the accessibility of the His side chains to interact with these ions and therefore, their arrangement on the surface of the sheets, we studied their catalytic properties on the surface of the 2D materials. To this end, we selected the hydrolysis of *p*-NitroPhenol Acetate (***p*-NPA**), a common indicator of hydrolase activity (Figure 8).[114] Additionally, we also performed catalysis experiments in the presence of Zn^{2+} ions to exploit their coordination with the imidazole rings and evaluate their catalytic activity through a different mechanism.[115,116] This process was followed by evaluating the increase in absorbance at 400 nm as a result of the formation of p-nitrophenol (***p*-NP**).

As shown in Figure 9a, the solution of **4CP$_{1K}$-U-TPE** (20 μM) in HEPES at pH 8 catalyzed the ***p*-NPA** hydrolysis, with more than 8-fold increases in the hydrolysis rate after 10 min. Moreover, the addition of Zn^{2+} further accelerates this process, suggesting that the metal ion coordinates with His side chains in order to participate in the catalysis (Figure 9b, Figure S25b). Adjusting the concentration profiles to a second-order kinetic rate expression showed apparent kinetic constants in the order of 10^{-2} L M^{-1} s^{-1}. Remarkably, the presence of Zn^{2+} increased 1.7–1.5 times the apparent kinetic constants of **4CP$_{QSR}$-U-TPE**, **4CP$_{QRS}$-U-TPE** and **1CP$_{QRS}$-U-B** (Figure S25c,d and Table S1). Concentration-dependent experiment where then performed, keeping constant the concentration of ***p*-NPA** while changing the CP concentration in the presence of Zn^{2+} (Figure S25a). A linear dependence between the hydrolysis rate and the CP concentration was confirmed. This is consistent with the previously reported relationship between the hydrolysis rate of phenyl acetates and the imidazole concentration.[111] We performed this experiment in the presence of Zn^{2+} since in the experiments initially performed with the 50 μM solution of **4CP$_{1K}$-U-TPE** (50 μM) without the metal, a precipitation was observed when the reaction mixture was allowed to stand for additional time. HPLC-MS analysis of the resulting mixture (Figure S27 and S28) showed acetylation of the Lys side chain over time, suggesting that the nucleophilic character of the amino group could be involved in the acceleration of the hydrolysis of ***p*-NPA**. Moreover changes were found in the emission properties of **4CP$_{1k}$-U-TPE** over time, only a small reduction at the end of the process that could be correlated with the mentioned precipitation or the absorption of ***p*-NP** formed (Figure S25e).

To evaluate the role of the lysine side chain, a new peptide scaffold without the Lys in its sequence was designed: **4CP$_{QRS}$-U-TPE** (for details on the CP structure and synthesis, see the Supporting Information). In this case, Ser_8 and Lys_1 were replaced by Gln and Arg, respectively (Figure 9c). Gln was incorporated to simplify CP synthesis and enable the macrocyclization of the peptide while it is still linked to the resin. This is necessary because replacing Lys with Arg, to maintain the cationic nature of the nanosheets, eliminates the previous anchor point used for synthesizing cyclic peptides on solid supports. Thus, CP synthesis was initiated using the glutamic acid side chain (Fmoc-Glu-OAll) to attach to the Rink Amide resin.[92] After cleavage, this provides the aforementioned Gln residue. The resulting tetrapeptide-TPE hybrid exhibits similar self-assembly properties to previous derivatives (Figure S26), again corroborating the excellent

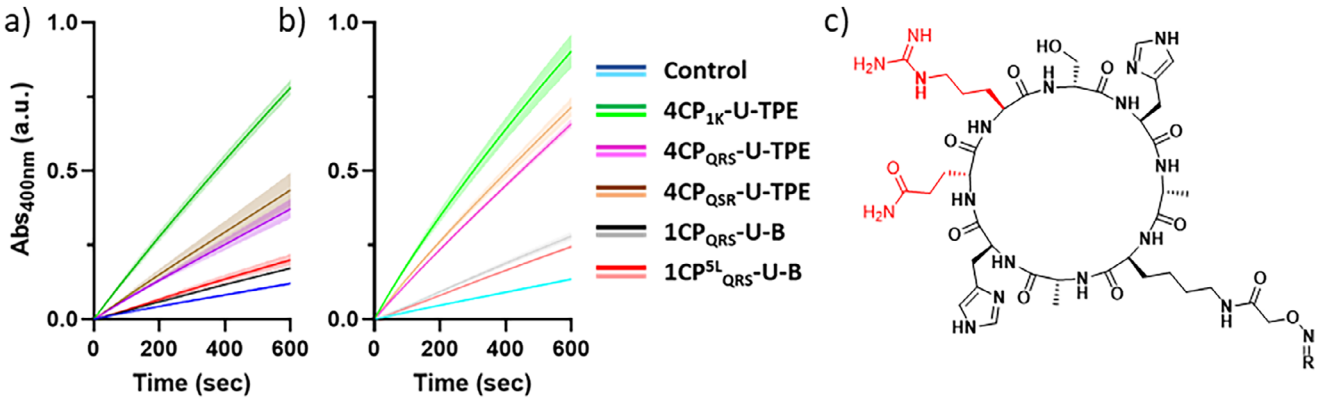

Figure 9. Catalytic activity of the different CPs derivatives (**4CPn-U-TPE** 20 μM and **1CPn-U-B** – 80 μM) at pH 8 in the presence of ***p*-NPA** (1 mM) in the a) absence and b) presence of 4.5 equivalents of Zn^{2+} (light shading represents the standard deviation from three independent measurements). c) General structures of $\mathbf{CP_{QRS}}$ derivatives.

templating effect of this design for the hierarchical assembly of AIE sheets in which the spatial arrangement of the different side chains is determined by the CP sequence (Figure 9a and b). Although the catalytic activity was lower than that of the Lys derivative, ***p*-NPA** hydrolysis experiments again showed an appreciable increase in the reaction rate for the assembled $\mathbf{4CP_{QRS}}$**-U-TPE**. However, the HPLC-MS analysis of these samples showed again the partial acetylation of the Ser moiety (Figure S28c and d). In view of these results, we decided to prepare a new derivative ($\mathbf{4CP_{QSR}}$**-U-TPE**) in which the positions of Arg and Ser were swapped, in order to move the serine side chain away from the catalytic space. Once again, the tetrakis-(cyclopeptide)TPE derivative assemble into the corresponding nanosheets, which were also capable of accelerating the hydrolysis of ***p*-NPA** in a manner analogous to the previous regioisomer. To our surprise, acetylation of the Ser side chain was also observed (Figure 9a,b and Figure S29).

Therefore, to clarify the reaction mechanisms, we decided to extend the reaction time to 1 h, following the formation of ***p*-NPA** by UV-vis while taking small aliquots of the reaction mixture to evaluate the acetylation pattern by HPLC-MS (Figure 10 and Figure S27, S28). Considering the initial reaction rates, all catalysts should be consumed within this time (1 h) if acetylation of the CPs were primarily responsible for the observed catalysis. In this case, a drastic reduction in the reaction rates should be observed once the nucleophilic groups of the peptides are consumed. As illustrated in Figure 9a and 9b, there is a clear difference in the initial hydrolysis rates between the two peptides, which becomes less pronounced at longer reaction times (Figure 10a). This suggests that the difference in rates observed at shorter reaction times could be due to the greater nucleophilicity of the amino group of Lys (Figure 10a, Figure S25b). We also confirmed that $\mathbf{4CP_{QRS}}$**-U-TPE** is only partially acetylated after 1 h of reaction, while more than one equivalent of ***p*-NPA** is consumed per Ser (Figure 10b). Therefore, the ratio between the equivalents of ***p*-NPA** consumed and Ser acetylated ($r < 1$) unambiguously validates the supramolecular catalysis, regardless of the results of acetylation, which would take place by a different mechanism (Figure 10b). Similar conclusions can be drawn from the analysis of the reaction catalyzed by $\mathbf{4CP_{1K}}$**-U-TPE**, however, in this case, up to twelve residues are susceptible to acetylation. Unfortunately, the acetylation of Lys causes a variation in the MS ionization of the products, making the quantitative analysis less precise (Figure S27 and S28).

Finally, to confirm the role played by the supramolecular structure, we synthetized two additional CP derivatives: $\mathbf{1CP_{QRS}}$**-U-B**, and $\mathbf{1CP^{5L}{}_{QRS}}$**-U-B** (for details on the CP structure and synthesis, see the Supporting Information). The control peptides $\mathbf{1CP_{QRS}}$**-U-B** and $\mathbf{1CP^{5L}{}_{QRS}}$**-U-B** were designed to reduce self-assembling properties by condensing the corresponding CPs with benzaldehyde. The first one, as expected had reduced assembly capabilities (CAC > 125 μM). The second derivative composed of five consecutive L-amino acids cannot adopt the required flat conformation required for stacking remaining in solution as a monomer (Figure S30). As expected, both control peptides showed reduced catalytic activity that hardly differed from the controls without CPs (Figure 9a,b), confirming the catalytic role of the supramolecular ordering of imidazole rings along the surface of the nanosheets. This conclusion is also consistent with the related carbonic anhydrase activity which requires three imidazole rings coordinated with metal center for its catalysis.[117] Taken together, these data demonstrate that the **4CP-U-TPE** hybrid scaffolds displaying histidine residues at the interface between nanosheets and the bulk water can act as efficient hydrolases.

Conclusion

In summary, here we have presented a novel cyclic peptide scaffold capable of hierarchically self-assembling into 2D supramolecular structures with aggregation-induced emission properties. The scaffold is based on a TPE moiety functionalized with four cyclic octapeptides of alternating chirality containing His residues as pH dependent assembling modulators. This new molecular scaffold self-assembles through the combination of β-sheet interactions, π–π stacking and hydrophobic effects, propagating the individual supramolecular properties of the basic components through a hierarchical supramolecular process. Furthermore, the

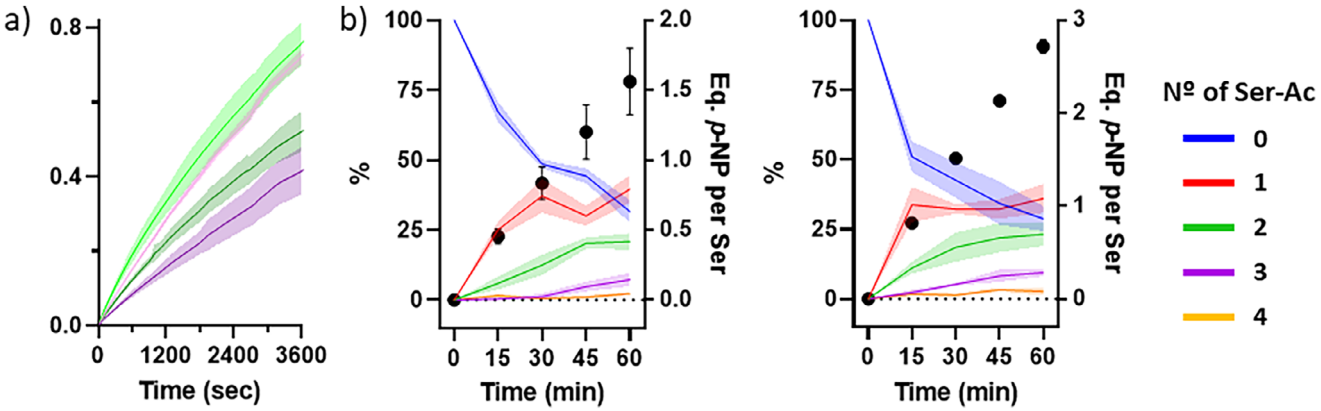

Figure 10. a) Catalytic activity of peptides **4CP$_{1K}$-U-TPE** (green) and **4CP$_{QRS}$-U-TPE** (purple) at 20 μM (HEPES 20 mM, pH 8) in the presence of ***p*-NPA** (1 mM) in the absence (dark lines) and presence of 4.5 equivalents Zn^{2+} (light lines). b) Acetylation pattern of **4CP$_{QRS}$-U-TPE** (lines) in the absence (left) and presence of Zn^{2+} (right) checked by HPLC-MS and the corresponding equivalents of ***p*-NPA** hydrolyzed at the corresponding times determined by the absorbance at 400 nm – and an $\varepsilon = 16\,600\ M^{-1}cm^{-1}$ described elsewhere [109] (black dots). The light shading represents the standard deviation from three independent measurements.

aggregation-induced emission properties of the TPE core provides an intrinsic fluorescent read-out that self-reports on thermal and pH responsiveness of the system. The characterization of the final assembly showed the formation of 2D materials in which the CPs, stacked in nanotubes, covered both sides of the supramolecular sheet while the TPE scaffold is located at the core of the assembly and arranged almost perpendicular to the programming axis of the nanotubes and sheets. Most importantly, this new building block tolerates a wide range of modifications to both the core TPE and the surrounding CPs without compromising the final 2D assembly mode. Structural modifications of the hydrophobic TPE core enable the first molecular-based design strategy that allows precise thickness control of 2D supramolecular architectures. Furthermore, we also show how this new class of peptide supramolecular materials can emulate the catalytic activity of enzymatic systems such as esterases or carbonic anhydrases, when Zn^{2+} metal ions are added. Taken together, the different imaging and spectroscopic characterization experiments presented here confirm that the tetrafunctionalization of a TPE moiety with cyclic peptides of alternating chirality constitutes a versatile strategy for the preparation of new biocompatible 2D supramolecular systems with precise thickness control, ordered aromatic cores and customized functional organic surfaces for multiple applications. We anticipate that this new approach to constructing 2D nanosheets with AIE properties will create new opportunities for developing self-reporting or photocatalytic active systems in which identification of the active structure could be detected and/or activated through the emission properties upon aggregation.

Acknowledgements

This work was supported by the Spanish Agencia Estatal de Investigación (AEI) (PID2022-142440NB-I00, PID2023-152181OB-I00), and by the Xunta de Galicia (ED431C 2021/21, ED431C 2024–03, ED431C 2025/15, the Oportunius Program (GAIN), the Centro de investigación do Sistema universitario de Galicia accreditation 2024–2027, ED431G 2023/03), and the European Union (European Regional Development Fund - ERDF). We also thank the ORFEO-CINCA network and Mineco (RED2022-134287-T). A. B.-F. and A. T.-C. thank Xunta de Galicia for their predoctoral contracts (ED481A-2019/085 and ED481A-2023–083). A. M.-A. supported the Ministry of Science and Innovation/State Research Agency (RYC2021-034263-I) and the European Union "NextGenerationEU/Recovery, Transformation and Resilience Plan" (10.13039/501100011033). M.C. and S.U. thank the ANR for the funding of the SelfBioMat project (ANR-17-CE07-0042-01). We acknowledge Jose M. Valpuesta, Noelia Zamarreño and M. Teresa Bueno for assistance in sample preparation and data acquisition at the CryoEM Facility CNB-CSIC, supported by the "Severo Ochoa" Programme for Centres of Excellence in R&D (CEX2023-001386-S).

Conflict of Interests

The authors declare no conflict of interest.

Data Availability Statement

The data that support the findings of this study are available from the corresponding author upon reasonable request.

Keywords: 2D Materials · Aggregation-induced Emission · Catalysis · Cyclic Peptides · Self-assembly

[1] K. S. Novoselov, A. K. Geim, S. V. Morozov, D. Jiang, Y. Zhang, S. V. Dubonos, I. V. Grigorieva, A. A. Firsov, *Science* **2004**, *306*, 666–669, https://doi.org/10.1126/science.1102896.

[2] X. Zhuang, Y. Mai, D. Wu, F. Zhang, X. Feng, *Adv. Mater.* **2015**, *27*, 403–427, https://doi.org/10.1002/adma.201401857.

[3] C. E. Boott, A. Nazemi, I. Manners, *Angew. Chem. Int. Ed.* **2015**, *54*, 13876–13894, https://doi.org/10.1002/anie.201502009.

[4] T. Govindaraju, M. B. Avinash, *Nanoscale* **2012**, *4*, 6102, https://doi.org/10.1039/c2nr31167d.

[5] I. Insua, J. Bergueiro, A. Méndez-Ardoy, I. Lostalé-Seijo, J. Montenegro, *Chem. Sci.* **2022**, *13*, 3057–3068, https://doi.org/10.1039/D1SC05667K.

[6] L. Gallego, J. F. Woods, M. Rickhaus, *Organic Mater.* **2022**, *4*, 137–145.

[7] I. W. Hamley, A. Dehsorkhi, V. Castelletto, *Chem. Commun.* **2013**, *49*, 1850, https://doi.org/10.1039/c3cc39057h.

[8] J. Lee, I. R. Choe, N. K. Kim, W. J. Kim, H. S. Jang, Y. S. Lee, K. T. Nam, *ACS Nano* **2016**, *10*, 8263–8270, https://doi.org/10.1021/acsnano.6b00646.

[9] H. V. Zhang, F. Polzer, M. J. Haider, Y. Tian, J. A. Villegas, K. L. Kiick, D. J. Pochan, J. G. Saven, *Sci. Adv.* **2016**, *2*, e1600307.

[10] E. L. Magnotti, S. A. Hughes, R. S. Dillard, S. Wang, L. Hough, A. Karumbamkandathil, T. Lian, J. S. Wall, X. Zuo, E. R. Wright, V. P. Conticello, *J. Am. Chem. Soc.* **2016**, *138*, 16274–16282, https://doi.org/10.1021/jacs.6b06592.

[11] U. Lewandowska, W. Zajaczkowski, S. Corra, J. Tanabe, R. Borrmann, E. M. Benetti, S. Stappert, K. Watanabe, N. A. K. Ochs, R. Schaeublin, C. Li, E. Yashima, W. Pisula, K. Müllen, H. Wennemers, *Nat. Chem.* **2017**, *9*, 1068–1072, https://doi.org/10.1038/nchem.2823.

[12] Y. Lin, M. Penna, M. R. Thomas, J. P. Wojciechowski, V. Leonardo, Y. Wang, E. T. Pashuck, I. Yarovsky, M. M. Stevens, *ACS Nano* **2019**, *13*, 1900–1909.

[13] H. S. Jang, J. H. Lee, Y. S. Park, Y. O. Kim, J. Park, T. Y. Yang, K. Jin, J. Lee, S. Park, J. M. You, K. W. Jeong, A. Shin, I. S. Oh, M. K. Kwon, Y. Il Kim, H. H. Cho, H. N. Han, Y. Kim, Y. H. Chang, S. R. Paik, K. T. Nam, Y. S. Lee, *Nat. Commun.* **2014**, *5*, 3665.

[14] B. Dai, D. Li, W. Xi, F. Luo, X. Zhang, M. Zou, M. Cao, J. Hu, W. Wang, G. Wei, Y. Zhang, C. Liua, *Proc. Natl. Acad. Sci. USA* **2015**, *112*, 2996–3001, https://doi.org/10.1073/pnas.1416690112.

[15] Y. Lin, M. R. Thomas, A. Gelmi, V. Leonardo, E. T. Pashuck, S. A. Maynard, Y. Wang, M. M. Stevens, *J. Am. Chem. Soc.* **2017**, *139*, 13592–13595.

[16] T. Kim, J. Hong, J. Kim, J. Cho, Y. Kim, *J. Am. Chem. Soc.* **2023**, *145*, 1793–1802, https://doi.org/10.1021/jacs.2c10938.

[17] I. Insua, J. Montenegro, *J. Am. Chem. Soc.* **2020**, *142*, 300–307, https://doi.org/10.1021/jacs.9b10582.

[18] S. Díaz, I. Insua, G. Bhak, J. Montenegro, *Chem. - Eur. J.* **2020**, *26*, 14765–14770.

[19] E. J. Robertson, G. K. Oliver, M. Qian, C. Proulx, R. N. Zuckermann, G. L. Richmond, *Proc. Natl. Acad. Sci. USA* **2014**, *111*, 13284–13289, https://doi.org/10.1073/pnas.1414843111.

[20] H. Jin, F. Jiao, M. D. Daily, Y. Chen, F. Yan, Y. H. Ding, X. Zhang, E. J. Robertson, M. D. Baer, C. L. Chen, *Nat. Commun.* **2016**, *7*, 12252.

[21] E. J. Robertson, A. Battigelli, C. Proulx, R. V. Mannige, T. K. Haxton, L. Yun, S. Whitelam, R. N. Zuckermann, *Acc. Chem. Res.* **2016**, *49*, 379–389, https://doi.org/10.1021/acs.accounts.5b00439.

[22] K. T. Nam, S. A. Shelby, P. H. Choi, A. B. Marciel, R. Chen, L. Tan, T. K. Chu, R. A. Mesch, B. C. Lee, M. D. Connolly, C. Kisielowski, R. N. Zuckermann, *Nat. Mater.* **2010**, *9*, 454–460, https://doi.org/10.1038/nmat2742.

[23] A. Battigelli, J. H. Kim, D. C. Dehigaspitiya, C. Proulx, E. J. Robertson, D. J. Murray, B. Rad, K. Kirshenbaum, R. N. Zuckermann, *ACS Nano* **2018**, *12*, 2455–2465, https://doi.org/10.1021/acsnano.7b08018.

[24] T. Jiang, C. Xu, X. Zuo, V. P. Conticello, *Angew. Chem. Int. Ed.* **2014**, *53*, 8367–8371, https://doi.org/10.1002/anie.201403780.

[25] T. Jiang, C. Xu, Y. Liu, Z. Liu, J. S. Wall, X. Zuo, T. Lian, K. Salaita, C. Ni, D. Pochan, V. P. Conticello, *J. Am. Chem. Soc.* **2014**, *136*, 4300–4308, https://doi.org/10.1021/ja412867z.

[26] A. S. Parmar, J. K. James, D. R. Grisham, D. H. Pike, V. Nanda, *J. Am. Chem. Soc.* **2016**, *138*, 4362–4367, https://doi.org/10.1021/jacs.5b10304.

[27] A. D. Merg, G. Touponse, E. van Genderen, X. Zuo, A. Bazrafshan, T. Blum, S. Hughes, K. Salaita, J. P. Abrahams, V. P. Conticello, *Angew. Chem. Int. Ed.* **2019**, *58*, 13507–13512, https://doi.org/10.1002/anie.201906214.

[28] T. P. J. Knowles, T. W. Oppenheim, A. K. Buell, D. Y. Chirgadze, M. E. Welland, *Nat. Nanotechnol.* **2010**, *5*, 204–207, https://doi.org/10.1038/nnano.2010.26.

[29] J. D. Brodin, J. R. Carr, P. A. Sontz, F. A. Tezcan, *Proc. Natl. Acad. Sci. USA* **2014**, *111*, 2897–2902, https://doi.org/10.1073/pnas.1319866111.

[30] S. Zhang, J. Zhang, W. Fang, Y. Zhang, Q. Wang, J. Jin, *Nano Lett.* **2018**, *18*, 6563–6569, https://doi.org/10.1021/acs.nanolett.8b03155.

[31] W. Bai, C. J. Sargent, J. M. Choi, R. V. Pappu, F. Zhang, *Nat. Commun.* **2019**, *10*, 3317.

[32] W. Liu, H. Zhong, R. Wang, N. C. Seeman, *Angew. Chem. Int. Ed.* **2011**, *50*, 264–267, https://doi.org/10.1002/anie.201005911.

[33] H. Yu, D. T. L. Alexander, U. Aschauer, R. Häner, *Angew. Chem. Int. Ed.***2017**, *56*, 5040–5044, https://doi.org/10.1002/anie.201701342.

[34] H. Jun, F. Zhang, T. Shepherd, S. Ratanalert, X. Qi, H. Yan, M. Bathe, *Sci. Adv.* **2019**, *5*, eaav0655.

[35] X. Wang, H. Jun, M. Bathe, *J. Am. Chem. Soc.* **2022**, *144*, 4403–4409, https://doi.org/10.1021/jacs.1c11332.

[36] Y. He, Y. Chen, H. Liu, A. E. Ribbe, C. Mao, *J. Am. Chem. Soc.* **2005**, *127*, 12202–12203, https://doi.org/10.1021/ja0541938.

[37] P. Wang, S. Gaitanaros, S. Lee, M. Bathe, W. M. Shih, Y. Ke, *J. Am. Chem. Soc.* **2016**, *138*, 7733–7740, https://doi.org/10.1021/jacs.6b03966.

[38] B. Yu, X. Jiang, J. Yin, *Macromolecules* **2014**, *47*, 4761–4768, https://doi.org/10.1021/ma500845e.

[39] H. Qiu, Y. Gao, C. E. Boott, O. E. C. Gould, R. L. Harniman, M. J. Miles, S. E. D. Webb, M. A. Winnik, I. Manners, *Science* **2016**, *352*, 697–701, https://doi.org/10.1126/science.aad9521.

[40] X. He, M. S. Hsiao, C. E. Boott, R. L. Harniman, A. Nazemi, X. Li, M. A. Winnik, I. Manners, *Nat. Mater.* **2017**, *16*, 481–488, https://doi.org/10.1038/nmat4837.

[41] M. Inam, G. Cambridge, A. Pitto-Barry, Z. P. L. Laker, N. R. Wilson, R. T. Mathers, A. P. Dove, R. K. O'Reilly, *Chem. Sci.* **2017**, *8*, 4223–4230, https://doi.org/10.1039/C7SC00641A.

[42] A. Nazemi, X. He, L. R. Macfarlane, R. L. Harniman, M. S. Hsiao, M. A. Winnik, C. F. J. Faul, I. Manners, *J. Am. Chem. Soc.* **2017**, *139*, 4409–4417, https://doi.org/10.1021/jacs.6b12503.

[43] L. Han, M. Wang, X. Jia, W. Chen, H. Qian, F. He, *Nat. Commun.* **2018**, *9*, 865, https://doi.org/10.1038/s41467-018-03195-y.

[44] J. Sun, Z. Wang, C. Zhu, M. Wang, Z. Shi, Y. Wei, X. Fu, X. Chen, R. N. Zuckermann, *Proc. Natl. Acad. Sci. USA* **2020**, *117*, 31639–31647, https://doi.org/10.1073/pnas.2011816117.

[45] A. Rajak, A. Das, *Angew. Chem. Int. Ed.***2022**, *61*, e202116572, https://doi.org/10.1002/anie.202116572.

[46] S. T. Wu, L. S. Long, R. Bin Huang, L. S. Zheng, *Cryst. Growth Des.* **2007**, *7*, 1746–1752, https://doi.org/10.1021/cg0608965.

[47] M. Kawaura, T. Aizawa, S. Takahashi, H. Miyasaka, H. Sotome, S. Yagai, *Chem. Sci.* **2022**, *13*, 1281–1287, https://doi.org/10.1039/D1SC06246H.

[48] J. Dong, L. Liu, C. Tan, Q. Xu, J. Zhang, Z. Qiao, D. Chu, Y. Liu, Q. Zhang, J. Jiang, Y. Han, A. P. Davis, Y. Cui, *Nature* **2022**, *602*, 606–611, https://doi.org/10.1038/s41586-022-04407-8.

[49] Q. Zhang, R. J. Xing, W. Z. Wang, Y. X. Deng, D. H. Qu, H. Tian, *iScience* **2019**, *19*, 14–24.
[50] A. Lampel, R. V. Ulijn, T. Tuttle, *Chem. Soc. Rev.* **2018**, *47*, 3737–3758, https://doi.org/10.1039/C8CS00177D.
[51] M. Coste, E. Suárez-Picado, S. Ulrich, *Chem. Sci.* **2022**, *13*, 909–933, https://doi.org/10.1039/D1SC05589E.
[52] I. Insua, A. Cardellini, S. Díaz, J. Bergueiro, R. Capelli, G. M. Pavan, J. Montenegro, *Chem. Sci.* **2023**, *14*, 14074–14081, https://doi.org/10.1039/D3SC03930G.
[53] J. Luo, Z. Xie, Z. Xie, J. W. Y. Lam, L. Cheng, H. Chen, C. Qiu, H. S. Kwok, X. Zhan, Y. Liu, D. Zhu, B. Z. Tang, *Chem. Commun.* **2001**, *18*, 1740–1741, https://doi.org/10.1039/b105159h.
[54] J. Mei, Y. Hong, J. W. Y. Lam, A. Qin, Y. Tang, B. Z. Tang, *Adv. Mater.* **2014**, *26*, 5429–5479, https://doi.org/10.1002/adma.201401356.
[55] Y. Tu, Z. Zhao, J. W. Y. Lam, B. Z. Tang, *Natl. Sci. Rev.* **2021**, *8*, nwaa260, https://doi.org/10.1093/nsr/nwaa260.
[56] Q. Peng, Z. Shuai, *Aggregate* **2021**, *2*, e91.
[57] Z. Zhao, H. Zhang, J. W. Y. Lam, B. Z. Tang, *Angew. Chem. Int. Ed.* **2020**, *59*, 9888–9907, https://doi.org/10.1002/anie.201916729.
[58] M. Wang, G. Zhang, D. Zhang, D. Zhu, B. Z. Tang, *J. Mater. Chem.* **2010**, *20*, 1858, https://doi.org/10.1039/b921610c.
[59] Y. Hong, J. W. Y. Lam, B. Z. Tang, *Chem. Soc. Rev.* **2011**, *40*, 5361, https://doi.org/10.1039/c1cs15113d.
[60] Y. Zuo, H. Shen, F. Sun, P. Li, J. Sun, R. T. K. Kwok, J. W. Y. Lam, B. Z. Tang, *ACS Bio. and Med. Chem. Au.* **2022**, *2*, 236–257, https://doi.org/10.1021/acsbiomedchemau.1c00066.
[61] M. Kang, Z. Zhang, N. Song, M. Li, P. Sun, X. Chen, D. Wang, B. Z. Tang, *Aggregate* **2020**, *1*, 80–106, https://doi.org/10.1002/agt2.7.
[62] J. Mei, N. L. C. Leung, R. T. K. Kwok, J. W. Y. Lam, B. Z. Tang, *Chem. Rev.* **2015**, *115*, 11718–11940, https://doi.org/10.1021/acs.chemrev.5b00263.
[63] Z. Zhao, J. W. Y. Lam, B. Z. Tang, *Curr. Org. Chem.* **2010**, *14*, 2109–2132, https://doi.org/10.2174/138527210793351571.
[64] T. Noguchi, T. Shiraki, A. Dawn, Y. Tsuchiya, L. T. Ngoc Lien, T. Yamamoto, S. Shinkai, *Chem. Commun.* **2012**, *48*, 8090, https://doi.org/10.1039/c2cc33262k.
[65] Y. Huang, F. Hu, R. Zhao, G. Zhang, H. Yang, D. Zhang, *Chem. - Eur. J.* **2014**, *20*, 158–164, https://doi.org/10.1002/chem.201303679.
[66] K. Liu, R. Zhang, Y. Li, T. Jiao, D. Ding, X. Yan, *Adv. Mater. Interfaces* **2017**, *4*, 1600183.
[67] M. Y. Yeh, C. W. Huang, J. W. Chang, Y. T. Huang, J. H. Lin, S. M. Hsu, S. C. Hung, H. C. Lin, *Soft Matter* **2016**, *12*, 6347–6351, https://doi.org/10.1039/C6SM00755D.
[68] S. K. Talloj, M. Mohammed, H. C. Lin, *J. Mater. Chem. B* **2020**, *8*, 7483–7493, https://doi.org/10.1039/D0TB01147A.
[69] E. Suárez-Picado, M. Coste, J. Y. Runser, M. Fosséprè, A. Carvalho, M. Surin, L. Jierry, S. Ulrich, *Biomacromolecules* **2022**, *23*, 431–442, https://doi.org/10.1021/acs.biomac.1c01389.
[70] Y. Wang, T. Pan, X. Wei, F. Su, A. Li, Y. Tai, T. Wei, Q. Zhang, D. Kong, C. Zhang, *Commun. Chem.* **2022**, *5*, 81, https://doi.org/10.1038/s42004-022-00700-9.
[71] Q. Liu, Q. Xia, S. Wang, B. S. Li, B. Z. Tang, *J. Mater. Chem. C* **2018**, *6*, 4807–4816, https://doi.org/10.1039/C8TC00838H.
[72] Z. Wang, X. He, T. Yong, Y. Miao, C. Zhang, B. Z. Tang, *J. Am. Chem. Soc.* **2020**, *142*, 512–519, https://doi.org/10.1021/jacs.9b11544.
[73] J. Chen, L. Chen, Y. Wu, Y. Fang, F. Zeng, S. Wu, Y. Zhao, *Nat. Commun.* **2021**, *12*, 6870, https://doi.org/10.1038/s41467-021-27233-4.
[74] J. Yang, X. Yu, J. I. Song, Q. Song, S. C. L. Hall, G. Yu, S. Perrier, *Angew. Chem. Int. Ed.* **2022**, *61*, e202115208, https://doi.org/10.1002/anie.202115208.
[75] W. Drożdż, C. Bouillon, C. Kotras, S. Richeter, M. Barboiu, S. Clément, A. R. Stefankiewicz, S. Ulrich, *Chem. - Eur. J.* **2017**, *23*, 18010–18018.
[76] M. Salimimarand, D. D. La, M. Al Kobaisi, S. V. Bhosale, *Sci. Rep.* **2017**, *7*, 42898, https://doi.org/10.1038/srep42898.
[77] E. Wang, J. W. Y. Lam, R. Hu, C. Zhang, Y. S. Zhao, B. Z. Tang, *J. Mater. Chem. C* **2014**, *2*, 1801, https://doi.org/10.1039/c3tc32161d.
[78] C. Kotras, M. Fosséprè, M. Roger, V. Gervais, S. Richeter, P. Gerbier, S. Ulrich, M. Surin, S. Clément, *Front. Chem.* **2019**, *7*, 493, https://doi.org/10.3389/fchem.2019.00493.
[79] Y. Wang, M. Lee, *ChemPlusChem* **2020**, *85*, 711–714, https://doi.org/10.1002/cplu.202000130.
[80] J. De, A. H. Abdul, R. A. K. Yadav, S. P. Gupta, I. Bala, P. Chawla, K. K. Kesavan, J. H. Jou, S. K. Pal, *Chem. Commun.* **2020**, *56*, 14279–14282, https://doi.org/10.1039/D0CC05813K.
[81] H. Shen, F. Sun, X. Zhu, J. Zhang, X. Ou, J. Zhang, C. Xu, H. H. Y. Sung, I. D. Williams, S. Chen, R. T. K. Kwok, J. W. Y. Lam, J. Sun, F. Zhang, B. Z. Tang, *J. Am. Chem. Soc.* **2022**, *144*, 15391–15402, https://doi.org/10.1021/jacs.2c07443.
[82] W. Z. Yuan, F. Mahtab, Y. Gong, Z. Q. Yu, P. Lu, Y. Tang, J. W. Y. Lam, C. Zhu, B. Z. Tang, *J. Mater. Chem.* **2012**, *22*, 10472, https://doi.org/10.1039/c2jm30620d.
[83] Z. Guo, G. Li, H. Wang, J. Zhao, Y. Liu, H. Tan, X. Li, P. J. Stang, X. Yan, *J. Am. Chem. Soc.* **2021**, *143*, 9215–9221, https://doi.org/10.1021/jacs.1c04288.
[84] J. Dong, K. Zhang, X. Li, Y. Qian, H. Zhu, D. Yuan, Q. H. Xu, J. Jiang, D. Zhao, *Nat. Commun.* **2017**, *8*, 1142, https://doi.org/10.1038/s41467-017-01293-x.
[85] D. D. La, S. V. Bhosale, L. A. Jones, S. V. Bhosale, *ACS Appl. Mater. Interfaces* **2018**, *10*, 12189–12216, https://doi.org/10.1021/acsami.7b12320.
[86] M. Nabara, S. Yamamoto, Y. Nishiyama, H. Nagatani, *Langmuir* **2020**, *36*, 10597–10605, https://doi.org/10.1021/acs.langmuir.0c01962.
[87] M. Coste, C. Kotras, Y. Bessin, V. Gervais, D. Dellemme, M. Leclercq, M. Fosséprè, S. Richeter, S. Clément, M. Surin, S. Ulrich, *Chem. - Eur. J.* **2021**, *2021*, 1123–1135, https://doi.org/10.1002/ejoc.202001420.
[88] Z. Zhao, J. W. Y. Lam, B. Z. Tang, *J. Mater. Chem.* **2012**, *22*, 23726, https://doi.org/10.1039/c2jm31949g.
[89] Y. Shi, S. Wang, W. Tao, J. Guo, S. Xie, Y. Ding, G. Xu, C. Chen, X. Sun, Z. Zhang, Z. He, P. Wei, B. Z. Tang, *Nat. Commun.* **2022**, *13*, 1882, https://doi.org/10.1038/s41467-022-29565-1.
[90] M. Coste, S. Ulrich, *Chem. Sci.* **2025**, https://doi.org/10.1039/D5SC04688B.
[91] F. B. L. Cougnon, A. R. Stefankiewicz, S. Ulrich, *Chem. Sci.* **2024**, *15*, 879–895, https://doi.org/10.1039/D3SC05343A.
[92] M. R. Ghadiri, J. R. Granja, R. A. Milligan, D. E. McRee, N. Khazanovich, *Nature* **1993**, *366*, 324–327, https://doi.org/10.1038/366324a0.
[93] Q. Song, Z. Cheng, M. Kariuki, S. C. L. Hall, S. K. Hill, J. Y. Rho, S. Perrier, *Chem. Rev.* **2021**, *121*, 13936–13995, https://doi.org/10.1021/acs.chemrev.0c01291.
[94] A. Fuertes, M. Juanes, J. R. Granja, J. Montenegro, *Chem. Commun.* **2017**, *53*, 7861–7871, https://doi.org/10.1039/C7CC02997G.
[95] J. Montenegro, M. R. Ghadiri, J. R. Granja, *Acc. Chem. Res.* **2013**, *46*, 2955–2965, https://doi.org/10.1021/ar400061d.
[96] A. Méndez-Ardoy, J. R. Granja, J. Montenegro, *Nanoscale Horiz.* **2018**, *3*, 391–396, https://doi.org/10.1039/C8NH00009C.
[97] A. Bayón-Fernández, A. Méndez-Ardoy, C. Alvarez-Lorenzo, J. R. Granja, J. Montenegro, *J. Mater. Chem. B* **2023**, *11*, 606–617, https://doi.org/10.1039/D2TB01721K.
[98] J. Guo, S. T. Rich-New, C. Liu, Y. Huang, W. Tan, H. He, M. Yi, X. Zhang, E. H. Egelman, F. Wang, B. Xu, *Chem* **2023**, *9*, 2530–2546, https://doi.org/10.1016/j.chempr.2023.04.023.

[99] A. Méndez-Ardoy, A. Bayón-Fernández, Z. Yu, C. Abell, J. R. Granja, J. Montenegro, *Angew. Chem. Int. Ed.* **2020**, *59*, 6902–6908, https://doi.org/10.1002/anie.202000103.
[100] L. S. Wolfe, M. F. Calabrese, A. Nath, D. V. Blaho, A. D. Miranker, Y. Xiong, *Proc. Natl. Acad. Sci. USA* **2010**, *107*, 16863–16868, https://doi.org/10.1073/pnas.1002867107.
[101] P. K. Singh, A. K. Mora, S. Nath, *Chem. Commun.* **2015**, *51*, 14042–14045, https://doi.org/10.1039/C5CC04256A.
[102] G. Gasparini, E. K. Bang, J. Montenegro, S. Matile, *Chem. Commun.* **2015**, *51*, 10389–10402, https://doi.org/10.1039/C5CC03472H.
[103] V. Castelletto, C. J. C. Edwards-Gayle, I. W. Hamley, G. Barrett, J. Seitsonen, J. Ruokolainen, *ACS Appl. Mater. Interfaces* **2019**, *11*, 9893–9903, https://doi.org/10.1021/acsami.9b00581.
[104] L. E. R. O'Leary, J. A. Fallas, E. L. Bakota, M. K. Kang, J. D. Hartgerink, *Nat. Chem.* **2011**, *3*, 821–828, https://doi.org/10.1038/nchem.1123.
[105] S.-M. Liao, J.-Z. Meng, Z.-W. Pang, R.-B. Huang, *Chem. Central J.* **2013**, *7*, 44, https://doi.org/10.1186/1752-153X-7-44.
[106] R. Calinsky, Y. Levy, *J. Chem. Theory Comput.* **2024**, *20*, 6930–6945, https://doi.org/10.1021/acs.jctc.4c00606.
[107] A. H. Iyer, R. N. V. Krishna Deepak, R. Sankararamakrishnan, *J. Phys. Chem. B* **2018**, *122*, 1205–1212, https://doi.org/10.1021/acs.jpcb.7b11737.
[108] J. Heyda, P. E. Mason, P. Jungwirth, *J. Phys. Chem. B* **2010**, *114*, 8744–8749, https://doi.org/10.1021/jp101031v.
[109] M. Hennig, B. H. Geierstanger, *J. Am. Chem. Soc.* **1999**, *121*, 5123–5126, https://doi.org/10.1021/ja990340o.
[110] Y. Zhao, B. Lei, M. Wang, S. Wu, W. Qi, R. Su, Z. He, *J. Mater. Chem. B* **2018**, *6*, 2444–2449, https://doi.org/10.1039/C8TB00448J.
[111] Q. Song, Z. Cheng, S. Perrier, *Polym. Chem.* **2023**, *14*, 4712–4718, https://doi.org/10.1039/D3PY00993A.
[112] M. Samanta, N. Saad, D. Wu, N. S. A. Crone, K. Abramov-Harpaz, C. Regev, R. Cohen-Luria, A. L. Boyle, Y. Miller, A. Kros, G. Ashkenasy, *Angew. Chem. Int. Ed.* **2025**, *64*, e202413810, https://doi.org/10.1002/anie.202413810.
[113] B. Sarkhel, A. Chatterjee, D. Das, *J. Am. Chem. Soc.* **2020**, *142*, 4098–4103, https://doi.org/10.1021/jacs.9b13517.
[114] C. Zhang, R. Shafi, A. Lampel, D. MacPherson, C. G. Pappas, V. Narang, T. Wang, C. Maldarelli, R. V. Ulijn, *Angew. Chem. Int. Ed.***2017**, *56*, 14511–14515, https://doi.org/10.1002/anie.201708036.
[115] L. Zhou, S. Li, Y. Su, X. Yi, A. Zheng, F. Deng, *J. Phys. Chem. B* **2013**, *117*, 8954–8965, https://doi.org/10.1021/jp4041937.
[116] D. Nakatake, Y. Yokote, Y. Matsushima, R. Yazaki, T. Ohshima, *Green Chem.* **2016**, *18*, 1524–1530, https://doi.org/10.1039/C5GC02056E.
[117] D. Vullo, F. Carta, in *Carbonic Anhydrases: Biochemistry and Pharmacology of an Evergreen Pharmaceutical Target*, Elsevier, London, England **2019**, pp. 187–222.

Manuscript received: July 07, 2025
Revised manuscript received: September 30, 2025
Manuscript accepted: October 15, 2025
Version of record online: November 10, 2025